

submitted to the Astronomical Journal October 25, 2018

High-Resolution Spectroscopy from 3050 to 10000 Å of the HDF-S QSO J2233-606 with UVES at the ESO VLT¹

S. Cristiani²

ST European Coordinating Facility, European Southern Observatory, D-85748 Garching bei München, Germany

and

V. D'Odorico

Institut d'Astrophysique de Paris, 98bis Bd Arago, F-75014 Paris

ABSTRACT

We report on high-resolution observations ($\mathfrak{R} \simeq 45000$) of the Hubble Deep Field South QSO J2233-606 obtained with the VLT UV-Visual Echelle Spectrograph (UVES). We present spectral data for the wavelength region $3050 < \lambda < 10000$ Å. The S/N ratio of the final spectrum is about 50 per resolution element at 4000 Å, 90 at 5000 Å, 80 at 6000 Å, 40 at 8000 Å. Redshifts, column densities and Doppler widths of the absorption features have been determined with Voigt-profile fitting. A total of 621 lines have been measured. In particular 270 Ly α lines, 41 Ly β and 24 systems containing metal lines have been identified. Together with other data in the literature, the present spectrum confirms that the evolution of the number density of Ly α lines with $\log N(\text{H I}) > 14$ has an upturn at $z \sim 1.4 - 1.6$.

Subject headings: cosmology: observations - quasars: absorption lines - quasars: individual (J2233-606)

1. Introduction

Starting on September 28, 1998 and for two weeks, the Hubble Space Telescope aimed at the same narrow slice of sky in the constellation Tucana. The observing strategy of the Hubble Deep Field South (HDF-S, Williams et al., 2000) differs from its northern analogous in several

¹Based on material collected with the ESO VLT telescope

²On leave from the Astronomy Department, University of Padua.

respects. The Space Telescope Imaging Spectrograph field was centered on a relatively bright ($B \simeq 17.5$) quasar at intermediate redshift (J2233-606, $z_{\text{em}} = 2.238$). The installation of STIS and NICMOS on HST in 1997 February has enabled parallel observations with three cameras. In this way the HDF-S dataset includes deep WFPC2 imaging (Casertano et al., 2000), UV-Visible imaging (Gardner et al., 2000) and spectroscopy (Savaglio et al., 1999), deep near-infrared imaging (Fruchter et al., 2000), and wider-area flanking field observations (Lucas et al., 2000). Ground-based observations have been carried out at ESO with the VLT and NTT telescopes in the framework of the ESO HDF-South Project (<http://www.eso.org/paranal/sv/svhdfs.html>). The simultaneous availability of deep imaging and a large spectroscopic coverage at medium-high resolution makes the HDF-S a unique field to study the relationship between galaxies and absorbers, the quasar environment, the abundance pattern of metal absorption systems.

Spectroscopic observations of J2233-606 have already been reported by Savaglio (1998, SAV98), Sealey et al. (1998), Outram et al. (1999, OUT99), and Savaglio et al. (1999). The relationship between the low redshift ($z \leq 1$) galaxies lying within 1' of the QSO and the absorption systems is described by Tresse et al. (1999), who also found another QSO in the field at an angular separation of 44.5" from the HDF-S QSO, with $z_{\text{em}} = 1.336$.

In this paper we present high-resolution spectroscopy ($\mathfrak{R} \simeq 45000$) carried out with the VLT UV-Visual Echelle Spectrograph, UVES (Dekker et al., 2000). These new data are unique in terms of S/N and spectral range (3050-10000 Å) and ideally match the HST STIS observations obtained in the interval 2275-3118 Å with a FWHM resolution of 10 km s⁻¹ (Savaglio et al., 1999). In Sect. 2 the observations and data reduction are described. Sect. 3 deals with the process of identification of the absorption lines and their fit through χ^2 minimization of Voigt profiles. In Sect. 4 the general properties of the Ly α forest are discussed, while Sect. 5 describes the 24 identified metal systems.

2. The Observations

The UVES observation of J2233-606 were carried out during the commissioning of the instrument in October 1999. Details are given in Table 1. Two set-ups were used: the first (dichroic 1) covering simultaneously the 3050-3875 Å and 4795-6815 Å ranges in the blue and red arm, respectively; the second (dichroic 2) covering simultaneously the 3760-5004 Å and 6725-10000 Å ranges in the blue and red arm, respectively.

The data have been reduced in the new UVES context available in the 99NOV edition of MIDAS, the ESO data reduction system. For the wavelength calibration Thorium lamp spectra have been used. Wavelengths have then been corrected to vacuum heliocentric values.

The final combined spectrum has been rebinned to a constant pixel size of 0.05 Å and covers the wavelength range $\lambda\lambda 3050 - 10000$ Å.

The resolution, as measured from the Thorium lines of the calibration spectra, extracted and treated in the same way as the QSOs spectra, is $\mathfrak{R} \simeq 45000$. The S/N ratio of the final spectrum is about 50 per resolution element at 4000 Å, 90 at 5000 Å, 80 at 6000 Å, 40 at 8000 Å.

The continuum level was established selecting regions apparently free of absorptions and then fitting a cubic spline with a large smoothness parameter. The normalized spectra were then spliced together to form a total spectrum.

A section of the normalized spectrum from 3100 to 4300 Å is shown in Fig. 1-2. The full spectrum is available in the form of FITS tables at the URL <http://www.stecf.org/hstprogrammes/J22/J22.html>.

3. Line identification and profile fitting

The MIDAS package FITLYMAN (Fontana & Ballester 1995) has been used to measure the parameters of the absorption lines. Line fitting through χ^2 minimization of Voigt profiles has been carried out in order to determine the redshifts, column densities and Doppler widths of the identified features. When possible, we based our fit on the components found for multiple ions at the same redshift. The absorption-line parameter fits are presented in Table 2. Heavy element systems are identified, in general, by the presence of the C IV and/or Mg II doublets. The spectral separation and intensity ratio between the lines of the doublet allow a firm identification. Subsequently, the strongest ions commonly observed in quasar spectra are searched for at the same redshift. The atomic parameters for the absorption lines observed in QSO spectra have been taken from Morton et al. (1991) and Verner, Barthel & Tytler (1994). All the lines not identified as metals in the Ly α forest are fitted as H I Ly α and Ly β .

If a strong ion is not detected in the spectrum, we report only an upper limit to the column density. The estimate is based on the fact that there is a linear relation between rest equivalent width and column density for weak lines (because they lie on the linear part of the curve of growth). First, the equivalent width limit for that region is computed and the corresponding column density is given by:

$$N_{\text{lim}}(\text{cm}^{-2}) \simeq 1.13 \times 10^{20} w_{\text{lim}}(\text{\AA}) / (\lambda_{\text{rest}}^2(\text{\AA}) \times f_{\text{osc}}). \quad (1)$$

4. The Ly α Forest

A total of 186 Ly α lines are observed in the interval $\lambda\lambda 3321.3 - 3885$ Å, i.e. between the onset of the Ly β forest and the range affected by the proximity effect. The HI column density distribution for $13 < \log N(\text{H I}) < 17.5$ is consistent with a power-law distribution with a slope -1.41 ± 0.05 , slightly flatter but not significantly different from the canonical value observed at

higher redshift (Giallongo et al. 1996). The Doppler parameter distribution peaks between 20-25 km s⁻¹, with a lower cutoff at 15 km s⁻¹ for lines with $\log N(\text{H I}) > 13$. Fig.3 shows the number density of Ly α lines with $\log N(\text{H I}) > 14$ observed in the spectrum of J2233-606. At a medium redshift $< z > = 1.96 \pm 0.23$ we observe 33 such lines, 14 of which are associated to metal systems (see below). The corresponding dn/dz is 71 ± 12 including metal systems and 41 ± 9 excluding metal systems. The previous estimate of the dn/dz in J2233-606 by Savaglio et al. (1999) is in good agreement with the present result. The comparison with data in the literature from other sight-lines, provides a consistent picture of the evolution of the density of Ly α absorbers with redshift. In particular, the measurement derived from the spectrum of J2233-606 is remarkably close to the HST point at $< z > = 1.6$ by Weymann et al. (1998), which is based on 19 lines observed in the spectrum of the QSO UM 18. Fig. 3 suggests that a sharp upturn in the density of Ly α lines with $\log N(\text{H I}) > 14$ takes place at a redshift $z = 1.4 - 1.6$.

The density of Ly α lines in J2233-606 not associated with metal systems (see next Section) is also shown in Fig. 3. The agreement with the corresponding data of Giallongo et al. (1996) is very good ³.

5. Metal systems

In general, we consider a group of absorption lines due to the same ion as an individual metal system when the components are blended or not separated by more than a few tens of km s⁻¹.

The strongest systems in the spectrum of J2233-606 were already detected by OUT99 and by SAV98. We started from their detections and looked for weaker components and more ions belonging to the same systems. Besides, we found 4 new Mg II doublets, 7 new C IV doublets and a new associated system showing C IV and N V absorptions.

In the following, we list the systems and give a short description of their main features. The quoted redshift is the one of the strongest component or the average redshift in the case of complex systems (i.e. more than three components).

All the metal systems are resumed in Table 3.

5.1. Intervening systems

5.1.1. System at $z_{\text{abs}} = -0.000002$

Strong Na I $\lambda\lambda 5891, 5897$ is seen from the interstellar medium of the Galaxy.

³ the definition of “Ly α line not associated with metal systems” is dependent on the data quality and is therefore not rigorous.

5.1.2. System at $z_{\text{abs}} = 0.0002$

The complex Ca II $\lambda\lambda 3934, 3969$ at this redshift was already observed by OUT99. We detected two more, weaker components. The $\lambda 3969$ line is blended with the N V $\lambda 1238$ feature at $z_{\text{abs}} = 2.206$.

5.1.3. System at $z_{\text{abs}} = 0.41426$

A single Mg II $\lambda\lambda 2796, 2803$ doublet occurs at this redshift (OUT99). The fit with one component yields a relatively poor result, since the equivalent width ratio of the first line, Mg II $\lambda 2796$, relative to the Mg II $\lambda 2803$ line is lower than expected. A fit with a double structure does not give a better result.

Tresse et al. (1999) observed three galaxies at $z \sim 0.4147$ in the 1' field around the quasar. They claim that another object, closer to the quasar and belonging to the same over-density of galaxies, could be the responsible for this absorption system.

5.1.4. System at $z_{\text{abs}} = 0.57017$

Tresse et al. (1999) found at a redshift $z = 0.57$ a late-type spiral galaxy at an impact parameter of $\sim 18 h^{-1}$ kpc⁴. HI absorption likely associated with this galaxy is seen in the Lyman series, the fit of the Lyman limit in the STIS spectrum gives $N(\text{H I}) \sim 10^{16.8} \text{ cm}^{-2}$.

The UVES spectrum shows the associated Mg II doublet, with the strongest component at $z_{\text{abs}} = 0.57017$. We fitted the system with three components, spanning $\sim 86 \text{ km s}^{-1}$.

5.1.5. System at $z_{\text{abs}} = 0.58008$

This new, two component Mg II doublet, seen in the UVES spectrum, falls at the redshift of another galaxy found in the field by Tresse et al. (1999) at an impact parameter $\sim 112 h^{-1}$ kpc from the quasar line of sight.

5.1.6. System at $z_{\text{abs}} = 0.64498$

A galaxy at a redshift $z = 0.6465$ was observed at an impact parameter $\sim 220 h^{-1}$ kpc from the quasar line of sight by Tresse et al. (1999). The UVES spectrum shows a single Mg II doublet

⁴ We consider $h = H_0/100 \text{ km/s/Mpc}$ and $q_0 = 0.5$

at this slightly lower absorption redshift.

5.1.7. System at $z_{\text{abs}} = 0.75313$

A new Mg II doublet was found at this redshift in the UVES spectrum.

5.1.8. System at $z_{\text{abs}} = 1.09169$

New C IV $\lambda\lambda 1548, 1550$ system, fitted with two components.

5.1.9. System at $z_{\text{abs}} = 1.32153$

A new C IV doublet in the Ly α forest is observed at this redshift. There is one, clear, unblended component in both $\lambda 1548$ and $\lambda 1550$ lines. On the basis of the absence of the corresponding Lyman β line, we assumed that the whole feature is C IV $\lambda 1548$ and not H I Ly α and we fitted it with three components. We tentatively identified a feature showing the same velocity profile as C IV to be the Si IV $\lambda 1393$ absorption, while the corresponding Si IV $\lambda 1402$ line is blended with a strong H I Ly α complex. At a slightly higher redshift, a weak Mg II doublet has been observed showing two stronger components and a flat one in Mg II $\lambda 2796$. At this redshift, also the lines of Fe II $\lambda 2600$, Fe II $\lambda 2382$, C II $\lambda 1334$, Si II $\lambda 1526$ have been detected.

5.1.10. System at $z_{\text{abs}} = 1.3368$

Tresse et al. (1999) found another quasar in the field at a redshift $z \simeq 1.3360$ and at an angular separation of $44.5''$ from the current object. They measured the H I column density from the Ly α and Ly β absorption lines, observed in the high resolution portion of the STIS spectrum. A one component fit gives $N(\text{H I}) \sim 5 \cdot 10^{15} \text{ cm}^{-2}$ and a Doppler parameter $b \sim 50 \text{ km s}^{-1}$.

The UVES spectrum reveals a complex C IV doublet absorption at a slightly higher redshift, covering almost 200 km s^{-1} . Even though the system falls in the Ly α forest, the identification is quite reliable due to the characteristic profile. The C IV $\lambda 1548$ feature is blended with the possible Si II $\lambda 1260$ of the system at $z_{\text{abs}} = 1.87$; while the reddest component of C IV $\lambda 1550$ could be blended with the possible N V $\lambda 1238$ at $z_{\text{abs}} = 1.926$. We detected also a weak, less extended Mg II doublet on the lower redshift side of the C IV absorption and a weak, possible Si IV doublet corresponding to the highest redshift component of C IV. Finally, a fit of the H I Ly α line in the STIS spectrum with the same velocity structure as the C IV system gives a total column density of $N(\text{H I}) \sim 3.7 \cdot 10^{16} \text{ cm}^{-2}$.

5.1.11. System at $z_{\text{abs}} = 1.4831$

A complex of five C IV $\lambda\lambda 1548, 1550$ doublets, spanning 75 km s^{-1} , is seen within the Ly α forest. The identification (by OUT99) is firm thanks to the distinctive pattern of the absorption. No other associated metal line is identified.

5.1.12. System at $z_{\text{abs}} = 1.5034$

We cannot confirm the existence of this system tentatively identified by SAV98.

The 3σ column density limit on the Mg II $\lambda 2796$ absorption is $N(\text{Mg II}) \lesssim 1.6 \times 10^{11} \text{ cm}^{-2}$. Other strong low ionization lines like Mg I $\lambda 2852$ and Fe II $\lambda 2382$ are not observed and there is not the expected strong Ly α line in the STIS spectrum.

5.1.13. System at $z_{\text{abs}} = 1.55635$

A new, possible, weak C IV doublet has been found at this redshift. The corresponding Ly α line has an unexpectedly low column density, $N(\text{H I}) \sim 8 \times 10^{13} \text{ cm}^{-2}$.

5.1.14. System at $z_{\text{abs}} = 1.59055$

This two component C IV doublet, separated by 9 km s^{-1} , was already observed by OUT99.

No Si IV absorption was detected for this system; $N(\text{Si IV}) \lesssim 4.3 \times 10^{11} \text{ cm}^{-2}$ is a 3σ upper limit on the column density. The UVES spectrum shows a possible N V doublet feature at the redshift of the stronger component. We fitted the corresponding Ly α line with the same components as the C IV doublet.

5.1.15. System at $z_{\text{abs}} = 1.73165$

A possible, weak C IV doublet has been found in the UVES spectrum, coinciding with a $N(\text{H I}) \simeq 1.2 \times 10^{14} \text{ cm}^{-2}$ Ly α line.

5.1.16. System at $z_{\text{abs}} = 1.78618$

This system was already reported by Sealey et al. (1998). C IV has been observed by SAV98 and by OUT99.

The UVES spectrum does not confirm the presence of Mg I $\lambda 2852$ tentatively detected by SAV98. The 3σ limit on this ion is $N(\text{Mg I}) \lesssim 7.2 \times 10^{10} \text{ cm}^{-2}$. On the other hand, the Si IV $\lambda\lambda 1393, 1402$ is visible in the Ly α forest, although there is clear blending with H I lines. The corresponding H I Ly α line was fitted with two components for a total column density, $N(\text{H I}) \simeq 3.5 \times 10^{15} \text{ cm}^{-2}$.

5.1.17. System at $z_{\text{abs}} = 1.81565$

At this redshift, a possible, extremely weak C IV doublet absorption is observed, the $\lambda 1550$ line is barely visible. We fitted the feature with two components, together with the corresponding H I Ly α line whose total column density is $N(\text{H I}) \simeq 1.4 \times 10^{15} \text{ cm}^{-2}$.

5.1.18. System at $z_{\text{abs}} = 1.8693$

This complex heavy element system was already reported by OUT99 and by SAV98.

The UVES spectrum, besides showing the Si IV $\lambda\lambda 1393, 1402$ doublet, partially resolves the C IV $\lambda\lambda 1548, 1550$ features and shows the associated absorption by Si III $\lambda 1206$. N V $\lambda 1238$ is blended with a H I Ly α , the 3σ limit on N V from the $\lambda 1242$ line is: $N \lesssim 3.4 \times 10^{12} \text{ cm}^{-2}$. As for the low ionization elements, the Mg II doublet is detected in correspondence of the high redshift components of Si IV and C II $\lambda 1334$, Si II $\lambda\lambda 1190, 1193, \lambda 1526, \lambda 1260$, Al II $\lambda 1670$ absorption are also present. $N(\text{Fe II}) \lesssim 4.3 \times 10^{11} \text{ cm}^{-2}$ is a 3σ limit on the column density of Fe II $\lambda 2382$. The H I Ly α line falls in the wavelength range of the UVES spectrum, the feature is heavily saturated. We obtained an acceptable fit with three components, even if the large values of the Doppler parameters and the velocity profiles of the metal absorptions suggest a more complex structure. We defer the analysis and discussion of this interesting system to a following paper (D'Odorico and Petitjean, 2000).

The Mg I $\lambda 2853$ absorption tentatively detected by SAV98, has been identified with a telluric line by comparing the spectrum with that of a standard star obtained at comparable resolution.

5.1.19. System at $z_{\text{abs}} = 1.92599$

A prominent Ly α was observed at this redshift in the UCLES spectrum (Outram et al., 1999).

In the UVES spectrum the C IV $\lambda\lambda 1548, 1550$ doublet is resolved. We fitted together C IV, Si IV $\lambda\lambda 1393, 1402$, and Si III $\lambda 1206$, with three components, spanning $\sim 60 \text{ km s}^{-1}$. The N V $\lambda 1238$ is blended with the C IV $\lambda 1550$ of the system at $z_{\text{abs}} = 1.337$. The possible weaker component is visible, while the existence of the stronger one is ruled out by the absence of the

corresponding N V λ 1242 line. As for the low ionization lines, they show a shift of -4 km s⁻¹ with respect to the strongest component of the high ionization absorptions. C II λ 1334 has been fitted with two components, while for Si II λ 1260 and a possible Mg II doublet, we fitted only the strongest one. The 3σ limit on the abundance of Fe II based on the absorption at λ 2382 is: $N(\text{Fe II}) \lesssim 4.9 \times 10^{11} \text{ cm}^{-2}$.

A simultaneous fit of H I Ly α , Ly β , Ly ϵ and Ly8 has been carried out.

5.1.20. System at $z_{\text{abs}} = 1.9422$

This system presents many ions of different elements at different ionization stages. OUT99 and SAV98 already detected the absorption due to C II λ 1334, Si II $\lambda\lambda$ 1260, 1304, Si III λ 1206, and Si IV $\lambda\lambda$ 1393, 1402, C IV $\lambda\lambda$ 1548, 1550, Mg II $\lambda\lambda$ 2796, 2803, Al III $\lambda\lambda$ 1854, 1862, C I λ 1560, respectively.

The higher resolution and signal-to-noise ratio of the UVES spectrum makes it possible to observe three new shallow components in C IV that are also present in H I Ly α . As for the strongest feature, C IV $\lambda\lambda$ 1548, 1550 and Si III λ 1206 are saturated and have been fitted following the velocity structure of Si IV $\lambda\lambda$ 1393, 1402. The 3σ limit on the N V column density is $N(\text{N V}) \lesssim 1.4 \times 10^{12} \text{ cm}^{-2}$. The H I Ly α , Ly γ , Ly ϵ and Ly10 lines have been fitted with the same velocity structure as the C IV doublet for a total column density of $N(\text{H I}) \sim 2 \times 10^{16} \text{ cm}^{-2}$ in agreement with the measurement by Prochaska and Burles (1999).

The low ionization lines C II λ 1334, Si II $\lambda\lambda$ 1190, 1193, λ 1260, λ 1304, λ 1526, Mg II $\lambda\lambda$ 2803, Al II λ 1670, and Al III λ 1854, have been detected and fitted with the same velocity profile. Mg II $\lambda\lambda$ 2796 was not considered in the fit because its strongest component is affected by the presence of a telluric absorption line. We do not confirm the existence of the C I $\lambda\lambda$ 1560 absorption tentatively identified by SAV98. $N(\text{Fe II}) \lesssim 3.8 \times 10^{11} \text{ cm}^{-2}$ is the 3σ limit on the abundance of Fe II based on the absorption at λ 2382.

A more complete discussion on these latter two interesting metal systems will appear in a further paper (D'Odorico and Petitjean, 2000).

5.1.21. System at $z_{\text{abs}} = 2.07728$

This weak C IV doublet was identified by SAV98.

We tentatively identified Si III λ 1206 and Fe II λ 2382 and a more reliable Si II λ 1260 absorption. The 3σ limit on the Si IV λ 1393 is: $N(\text{Si IV}) \lesssim 3.2 \times 10^{11} \text{ cm}^{-2}$ and that on C II λ 1334, $N(\text{C II}) \lesssim 1.3 \times 10^{12} \text{ cm}^{-2}$. Unfortunately, the possible Mg II $\lambda\lambda$ 2796, 2803 absorptions at this redshift fall in the gap between the two UVES red arm CCDs.

5.1.22. System at $z_{\text{abs}} = 2.11287$

New, weak C IV doublet fitted with two components. The corresponding H I Ly α line shows a column density $N(\text{H I}) \simeq 8.1 \times 10^{14} \text{ cm}^{-2}$.

5.2. Associated systems

The associated systems observed in the redshift range 2.198 – 2.206 have been investigated by Petitjean and Srianand (1999). They found that most of the lines in these systems show the signature of partial coverage and the covering factor varies from species to species. In general, absolute abundances are close to solar, with the exception of the [N/C] abundance ratio which is larger than solar. This result confirms the physical association of the absorbing gas with the AGN.

5.2.1. System at $z_{\text{abs}} = 2.19819$

This associated system shows a strong C IV doublet at about -2000 km s^{-1} from the emission peak. OUT99 detected and fitted the N V doublet and the H I Ly α absorption line.

In the UVES spectrum we found a third, shallow component on the lower redshift side. C IV $\lambda\lambda 1548, 1550$, N V $\lambda\lambda 1238, 1242$, O VI $\lambda\lambda 1031, 1037$, H I Ly α and H I Ly β have been fitted together. The result of the fit is quite unsatisfactory ($\chi^2 = 9.5$), due to the unusual ratio between the lines of the doublets. In particular, the O VI lines show a flat bottom - as if they were saturated - but a non zero residual flux, a clear signature of partial coverage. The 3σ limit on the Si IV $\lambda 1393$ is $N(\text{Si IV}) \lesssim 5.2 \times 10^{11} \text{ cm}^{-2}$.

5.2.2. System at $z_{\text{abs}} = 2.20106$

This new, broad and shallow system shows the N V $\lambda\lambda 1238, 1242$ and C IV $\lambda 1548$ lines. C IV $\lambda 1550$ and O VI $\lambda\lambda 1031, 1037$ are blended in the forest. The 3σ limit on H I, from the absence of detectable H I Ly α , is $N(\text{H I}) \lesssim 3.6 \times 10^{11} \text{ cm}^{-2}$.

5.2.3. System at $z_{\text{abs}} = 2.2064$

A multi-component, broad C IV absorption in the redshift range between about -1400 km s^{-1} and -1100 km s^{-1} from the emission peak was observed by SAV98. OUT99 fitted the N V $\lambda\lambda 1238, 1242$ and the H I Ly α with three components, the fit is complicated by uncertainty in the precise shape of the Ly α & N V emission line continuum, also, the N V $\lambda 1242$ from the $z_{\text{abs}} = 2.198$ system lay on top of the N V $\lambda 1238$.

We performed a simultaneous fit of the C IV, N V, O VI doublets and the H I Ly α with five components. The 3σ limit on the Si IV column density is $N(\text{Si IV}) \lesssim 3.3 \times 10^{11} \text{ cm}^{-2}$.

We are greatly indebted to all the people involved in the conception, construction and commissioning of the UVES instrument, without whom this project would have been impossible. We are grateful to the members of the ESO Data Management Division Pascal Ballester, Sebastian Wolff and Andrea Modigliani for the development of the MIDAS-based UVES pipeline which was used to reduce these data. We thank J. Bergeron, S. D'Odorico, T.-S. Kim and S. Savaglio for enlightening discussions. This work has been conducted with partial support by the TMR programme Formation and Evolution of Galaxies set up by the European Community under the contract FMRX-CT96-0086.

Table 1. Journal of the observations of J2233-606

Date	Wavelength Range Å	Dichroic	Exposure Time s
1999 Oct 08	3050-3875	DIC1	3600
1999 Oct 08	3050-3875	DIC1	3600
1999 Oct 11	3050-3875	DIC1	3000
1999 Oct 12	3050-3875	DIC1	3000
1999 Oct 12	3050-3875	DIC1	3000
1999 Oct 10	3760-5004	DIC2	2700
1999 Oct 10	3760-5004	DIC2	2700
1999 Oct 10	3760-5004	DIC2	3300
1999 Oct 16	3760-5004	DIC2	3600
1999 Oct 08	4795-6815	DIC1	3600
1999 Oct 08	4795-6815	DIC1	3600
1999 Oct 12	4795-6815	DIC1	3000
1999 Oct 12	4795-6815	DIC1	3000
1999 Oct 12	4795-6815	DIC1	3000
1999 Oct 10	6725-10000	DIC2	2700
1999 Oct 10	6725-10000	DIC2	2700
1999 Oct 10	6725-10000	DIC2	3300
1999 Oct 16	6725-10000	DIC2	3600

Table 2. Absorption-line parameter list

ID	λ_{rest} Å	λ_{obs} Å	σ_λ Å	redshift	$\log N$	$\sigma_{\log N}$	b km s $^{-1}$	σ_b km s $^{-1}$
H I	1025.72	3088.793	0.005	2.0113347	13.85	0.01	26.7	0.7
C II	1334.53	3098.358	0.003	1.3216810	12.7	0.5	2.7	0.6
C II	1334.53	3098.468	0.007	1.3217632	12.9	0.3	5	1
H I	1025.72	3102.299	0.008	2.0245020	14.08	0.04	22.2	0.9
H I*	1215.67	3107.89	0.05	1.5565236	13.89	0.05	54	5
H I*	1215.67	3109.77	0.05	1.5580728	13.70	0.06	50	5
H I	1215.67	3129.14	0.02	1.5740037	13.77	0.05	25	3
H I	1215.67	3130.33	0.06	1.5749855	13.50	0.06	49	8
H I	1215.67	3133.5	0.1	1.5776194	13.2	0.1	52	14
H I	1215.67	3135.12	0.02	1.5789280	14.19	0.06	34	3
H I	1025.72	3138.160	0.005	2.0594633	13.67	0.01	31.7	0.7
H I	1215.67	3141.07	0.06	1.5838194	13.58	0.05	55	8
H I	1215.67	3145.45	0.04	1.5874223	13.33	0.07	30	5
H I*	1215.67	3148.21	0.04	1.5896888	13.89	0.05	35	7
H I*	1215.67	3149.257	0.004	1.5905521	14.1	0.4	36	16
H I	1215.67	3149.45	0.01	1.5907099	15.2	0.4	28	4
H I	1025.72	3152.685	0.003	2.0736241	14.33	0.01	31.1	0.4
H I	1025.72	3153.522	0.007	2.0744402	13.52	0.07	18	1
H I	1025.72	3155.7	0.2	2.0765765	13.2	0.3	29	9
H I	1025.72	3156.10	0.08	2.0769508	15.2	0.2	21	3
H I	1025.72	3156.54	0.03	2.0773849	15.45	0.09	24.7	0.9
H I	1025.72	3158.762	0.004	2.0795488	14.62	0.06	16.2	0.5
H I	1215.67	3161.33	0.03	1.6004813	13.40	0.05	33	3
H I	1025.72	3166.434	0.004	2.0870287	13.92	0.01	28.3	0.4
H I	1215.67	3172.21	0.02	1.6094297	14.08	0.04	29	2
H I	1215.67	3173.39	0.02	1.6104041	14.7	0.2	36	6
H I	1215.67	3174.3	0.2	1.6111625	14.0	0.1	91	18
H I	1215.67	3181.5	0.1	1.6171044	13.0	0.1	50	13
H I	1025.72	3186.069	0.007	2.1061709	13.61	0.01	23.7	0.9
H I	1215.67	3186.92	0.04	1.6215378	12.9	0.1	19	4
H I	1215.67	3187.63	0.02	1.6221206	13.51	0.04	22	2
H I*	1025.72	3192.94	0.02	2.1128747	14.85	0.04	33.3	0.9
H I*	1025.72	3193.17	0.03	2.1130946	14.0	0.1	42	4
H I	1215.67	3199.19	0.02	1.6316259	13.38	0.04	24	2
H I	1215.67	3205.17	0.05	1.6365429	13.32	0.05	48	6
N V	1238.82	3209.231	0.000	1.5905524	13.20	0.08	14	3

Table 2—Continued

ID	λ_{rest}	λ_{obs}	σ_λ	redshift	$\log N$	$\sigma_{\log N}$	b	σ_b
	Å	Å	Å				km s ⁻¹	km s ⁻¹
H I	1215.67	3212.34	0.03	1.6424410	13.37	0.04	37	3
H I	1215.67	3216.18	0.04	1.6456063	13.03	0.06	31	5
N V	1242.80	3219.549	0.000	1.5905527	13.20	0.08	14	3
H I	1025.72	3227.658	0.007	2.1467171	13.42	0.01	26.3	0.8
H I	1215.67	3229.67	0.04	1.6567017	12.8	0.1	19	6
H I	1025.72	3230.12	0.02	2.1491137	13.4	0.1	22	1
H I	1025.72	3230.52	0.04	2.1495104	13.72	0.06	34	4
H I	1025.72	3231.194	0.007	2.1501646	13.69	0.02	20.1	0.8
Si IV	1393.75	3235.09	(f)	1.321131	12.4	0.1	16	6
Si IV	1393.75	3235.65	(f)	1.321536	13.19	0.04	28	3
H I	1215.67	3238.01	0.08	1.6635625	12.5	0.2	22	12
C IV	1548.19	3238.339	0.005	1.0916867	13.53	0.03	8.6	0.8
C IV	1550.77	3243.725	0.005	1.0916867	13.53	0.03	8.6	0.8
H I	1025.72	3252.346	0.002	2.1707866	13.81	0.01	22.9	0.3
H I	1215.67	3253.20	0.01	1.6760527	13.73	0.03	24	1
H I	1215.67	3255.22	0.02	1.6777151	13.44	0.05	23	2
H I	1215.67	3255.91	0.02	1.6782843	13.74	0.04	32	4
H I	1215.67	3256.86	0.01	1.6790679	14.09	0.04	28	2
Si IV	1393.76	3257.756	0.000	1.3373951	12.0	0.2	2	1
H I	1215.67	3263.38	0.01	1.6844269	13.25	0.03	19	1
H I	1215.67	3268.17	0.02	1.6883729	13.26	0.03	28	3
H I	1215.67	3270.42	0.04	1.6902214	12.83	0.07	23	4
H I	1215.67	3271.47	0.03	1.6910836	12.5	0.1	12	4
H I	1215.67	3276.88	0.09	1.6955346	14.4	0.2	45	4
H I	1215.67	3277.5	0.6	1.6960195	13.8	0.6	59	22
Si IV	1402.77	3278.827	0.000	1.3373948	12.0	0.2	2	1
H I	1025.72	3280.091	0.000	2.1978357	12.64	0.06	26	3
H I	1025.72	3280.463	0.000	2.1981976	13.59	0.01	36.4	0.7
H I	1215.67	3282.83	0.04	1.7004291	12.75	0.08	22	4
H I	1025.72	3284.95	0.07	2.2025692	13.5	0.2	38	3
H I	1025.72	3284.95	0.07	2.2025692	13.5	0.2	38	3
H I	1025.72	3285.22	0.02	2.2028329	13.87	0.08	32	1
H I	1215.67	3288.79	0.01	1.7053307	13.70	0.02	35	1
H I	1215.67	3293.33	0.01	1.7090638	13.25	0.03	21	2
H I	1215.67	3298.89	0.03	1.7136384	12.99	0.09	18	4
H I	1215.67	3299.14	0.02	1.7138437	12.8	0.1	7	2

Table 2—Continued

ID	λ_{rest}	λ_{obs}	σ_λ	redshift	$\log N$	$\sigma_{\log N}$	b	σ_b
	Å	Å	Å				km s ⁻¹	km s ⁻¹
O VI	1031.93	3299.36	0.01	2.1972859	13.79	0.05	13	1
O VI	1031.93	3299.927	0.005	2.1978328	13.4	0.3	7	3
O VI	1031.93	3300.302	0.002	2.1981955	15.10	0.03	39	1
H I	1215.67	3302.94	0.02	1.7169679	13.34	0.03	22	2
H I	1025.72	3303.85	0.02	2.2210007	13.57	0.04	24	1
H I	1215.67	3303.95	0.01	1.7178036	14.23	0.03	40	1
H I	1025.72	3304.48	0.02	2.2216101	13.80	0.06	36	5
H I	1025.72	3305.04	0.04	2.2221594	13.3	0.1	27	2
H I	1215.67	3305.51	0.02	1.7190884	13.29	0.03	34	3
O VI	1031.93	3307.570	0.009	2.2052388	14.95	0.01	77	2
O VI	1031.93	3308.386	0.007	2.2060297	13.96	0.07	29	3
O VI	1031.93	3309.23	0.01	2.2068520	14.26	0.04	43	4
O VI	1031.93	3309.98	0.02	2.2075779	14.29	0.03	46	3
H I	1215.67	3310.96	0.04	1.7235715	13.11	0.05	37	5
H I	1215.67	3312.43	0.01	1.7247777	13.44	0.02	25	1
O VI	1037.62	3317.56	0.01	2.1972859	13.79	0.05	13	1
O VI	1037.62	3318.125	0.005	2.1978328	13.4	0.3	7	3
O VI	1037.62	3318.501	0.002	2.1981955	15.10	0.03	39	1
H I	1215.67	3319.83	0.02	1.7308642	13.18	0.05	25	3
H I*	1215.67	3320.78	0.01	1.7316473	14.10	0.03	32	2
H I	1215.67	3321.34	0.09	1.7321060	13.4	0.2	31	14
H I	1215.67	3321.92	0.07	1.7325817	13.4	0.1	28	5
O VI	1037.62	3325.809	0.009	2.2052388	14.95	0.01	77	2
O VI	1037.62	3326.630	0.007	2.2060297	13.96	0.07	29	3
O VI	1037.62	3327.48	0.01	2.2068520	14.26	0.04	43	4
O VI	1037.62	3328.24	0.02	2.2075779	14.29	0.03	46	3
H I	1215.67	3342.20	0.02	1.7492701	14.10	0.02	48	2
H I	1215.67	3343.10	0.02	1.7500080	13.96	0.03	33	2
H I	1215.67	3347.49	0.01	1.7536141	13.27	0.02	21	1
H I	1215.67	3352.65	0.02	1.7578661	13.09	0.03	28	2
H I	1215.67	3360.381	0.008	1.7642213	13.77	0.01	24.1	0.9
H I	1215.67	3360.84	0.02	1.7646028	12.6	0.1	11	3
H I	1215.67	3361.53	0.01	1.7651631	13.30	0.02	25	1
H I	1215.67	3369.85	0.02	1.7720103	12.40	0.10	8	2
H I	1215.67	3374.73	0.01	1.7760248	13.06	0.03	17	1
H I	1215.67	3376.02	0.02	1.7770855	12.60	0.08	13	3

Table 2—Continued

ID	λ_{rest}	λ_{obs}	σ_λ	redshift	$\log N$	$\sigma_{\log N}$	b	σ_b
	Å	Å	Å				km s ⁻¹	km s ⁻¹
H I	1215.67	3377.94	0.03	1.7786627	13.00	0.04	30	3
H I*	1215.67	3387.13	0.03	1.7862233	15.5	0.2	33	2
H I*	1215.67	3388.28	0.04	1.7871722	14.5	0.1	32	3
H I	1215.67	3389.28	0.02	1.7879915	13.23	0.05	24	3
H I	1215.67	3390.25	0.01	1.7887923	12.98	0.04	15	1
H I	1215.67	3395.14	0.01	1.7928125	13.71	0.02	28	2
H I	1215.67	3395.76	0.06	1.7933209	13.5	0.2	18	5
H I	1215.67	3396.24	0.04	1.7937227	14.22	0.07	28	2
H I	1215.67	3398.45	0.02	1.7955393	12.66	0.08	11	3
H I	1215.67	3399.56	0.02	1.7964505	12.86	0.05	16	2
H I	1215.67	3401.421	0.005	1.7979808	14.11	0.02	26.4	0.7
H I	1215.67	3402.66	0.03	1.7989960	12.5	0.1	13	4
H I	1215.67	3403.38	0.06	1.7995954	12.5	0.1	26	7
H I	1215.67	3405.82	0.08	1.8016007	12.66	0.09	42	9
H I	1215.67	3408.508	0.004	1.8038100	15.28	0.08	35	1
H I	1215.67	3414.04	0.02	1.8083580	13.37	0.02	36	2
H I	1215.67	3415.53	0.03	1.8095878	12.3	0.1	12	3
Si II	1190.42	3416.58	(f)	1.8700753	12.09	0.09	5.3	(f)
H I	1215.67	3417.65	0.03	1.8113306	12.88	0.06	25	4
H I	1215.67	3420.63	0.01	1.8137847	13.26	0.02	19	1
H I*	1215.67	3422.49	0.02	1.8153124	14.8	0.1	36	2
H I*	1215.67	3422.90	0.02	1.8156518	14.9	0.1	40	2
Si II	1193.29	3424.83	(f)	1.8700753	12.09	0.09	5.3	(f)
H I	1215.67	3426.588	0.007	1.8186829	13.55	0.01	23.1	0.9
H I	1215.67	3427.37	0.03	1.8193241	12.81	0.07	22	4
H I	1215.67	3428.17	0.05	1.8199818	12.73	0.09	33	9
H I	1215.67	3430.79	0.03	1.8221408	13.03	0.04	27	3
H I	1215.67	3431.50	0.03	1.8227222	12.75	0.07	22	4
H I	1215.67	3432.470	0.008	1.8235209	13.43	0.02	25	1
H I	1215.67	3443.14	0.02	1.8323003	12.88	0.05	23	3
H I	1215.67	3444.88	0.01	1.8337336	13.14	0.03	23	2
H I	1215.67	3449.05	0.01	1.8371637	13.53	0.03	24	1
H I	1215.67	3449.8	0.2	1.8377728	12.7	0.2	44	19
H I	1215.67	3454.79	0.04	1.8418856	12.56	0.07	21	4
H I	1215.67	3456.87	0.04	1.8435938	12.44	0.09	19	4
H I	1215.67	3457.588	0.007	1.8441831	13.40	0.01	21.4	0.8

Table 2—Continued

ID	λ_{rest}	λ_{obs}	σ_λ	redshift	$\log N$	$\sigma_{\log N}$	b	σ_b
	Å	Å	Å				km s ⁻¹	km s ⁻¹
H I	1215.67	3459.35	0.01	1.8456312	12.67	0.05	9	1
Si III	1206.50	3459.632	(f)	1.8674945	12.66	0.04	5.1	0.4
Si III	1206.50	3459.937	(f)	1.8677472	11.93	0.05	5	1
H I	1215.67	3460.791	0.007	1.8468175	13.81	0.01	23.3	0.8
H I	1215.67	3461.24	0.01	1.8471848	12.76	0.07	9	2
Si III	1206.50	3462.374	(f)	1.8697671	13.09	0.05	8.4	0.5
Si III	1206.50	3462.745	(f)	1.8700747	13.01	0.07	6.5	0.5
Si III	1206.50	3462.935	(f)	1.8702321	12.13	0.06	6	1
Si III	1206.50	3463.151	(f)	1.8704110	11.84	0.08	6	1
Si III	1206.50	3463.357	(f)	1.8705817	12.24	0.07	5	1
H I	1215.67	3463.63	0.02	1.8491565	13.24	0.07	18	3
Si III	1206.50	3463.957	(f)	1.8710792	12.96	0.04	13	1
H I	1215.67	3464.40	0.03	1.8497853	12.94	0.08	19	4
Si III	1206.50	3464.822	(f)	1.8717961	11.5	0.1	3	1
H I	1215.67	3465.85	0.01	1.8509771	12.67	0.05	9	1
H I	1215.67	3467.299	0.005	1.8521709	14.13	0.02	26.0	0.6
H I	1215.67	3471.777	0.008	1.8558547	13.52	0.01	24.7	0.9
H I	1215.67	3478.740	0.007	1.8615828	13.94	0.01	43.7	0.8
H I	1215.67	3482.56	0.02	1.8647280	12.94	0.04	21	2
H I	1215.67	3483.287	0.008	1.8653228	13.42	0.02	22	1
H I	1215.67	3484.516	0.006	1.8663337	14.20	0.03	24.0	0.8
H I*	1215.67	3487.72	0.07	1.8689656	15.9	0.1	111	5
H I*	1215.67	3490.99	0.08	1.8716619	14.67	0.05	75	9
H I	1215.67	3492.35	0.03	1.8727814	14.6	0.1	28	2
H I	1215.67	3499.209	0.006	1.8784198	13.89	0.01	27.4	0.6
H I	1215.67	3502.50	0.06	1.8811278	12.89	0.06	42	8
Si II	1190.42	3502.927	0.004	1.9426085	12.59	0.04	5.5	0.6
H I	1215.67	3504.91	0.01	1.8831102	13.63	0.02	33	1
H I	1215.67	3506.1	0.1	1.8840972	13.0	0.1	60	17
H I	1215.67	3506.966	0.009	1.8848006	13.24	0.03	20	1
H I	1215.67	3509.13	0.01	1.8865831	13.24	0.02	28	1
Si II	1193.29	3510.65	0.02	1.941996	11.75	0.09	10	3
Si II	1193.29	3511.19	0.02	1.942445	12.57	0.05	19	2
Si II	1193.29	3511.384	0.003	1.9426085	12.59	0.04	5.5	0.6
H I	1215.67	3516.687	0.007	1.8927975	13.75	0.01	27.2	0.8
H I	1215.67	3518.297	0.006	1.8941215	13.69	0.01	24.8	0.6

Table 2—Continued

ID	λ_{rest}	λ_{obs}	σ_λ	redshift	$\log N$	$\sigma_{\log N}$	b	σ_b
	Å	Å	Å				km s ⁻¹	km s ⁻¹
H I	1215.67	3523.050	0.009	1.8980311	13.24	0.02	20	1
H I	1215.67	3526.12	0.02	1.9005538	13.35	0.02	34	2
H I	1215.67	3527.13	0.02	1.9013865	13.24	0.03	24	2
H I	1215.67	3527.80	0.04	1.9019353	12.81	0.08	25	5
Si III	1206.50	3529.53	0.04	1.9254285	11.7	0.2	11	5
Si III	1206.50	3529.88	0.01	1.925719	12.61	0.04	14	1
Si III	1206.5	3530.03	0.02	1.925839	11.8	0.3	5	3
Si III	1206.50	3530.206	0.002	1.9259890	12.76	0.09	6.7	0.2
H I	1215.67	3530.31	0.01	1.9040003	13.16	0.05	14	1
H I	1215.67	3540.98	0.04	1.9127812	12.59	0.07	20	4
Si II	1526.71	3544.526	0.004	1.3216810	12.1	0.3	2.7	0.6
Si II	1526.71	3544.651	0.008	1.3217630	12.6	0.1	5	1
Si III	1206.50	3549.493	0.005	1.9419751	12.70	0.03	14.3	0.7
Si III	1206.50	3549.525	0.003	1.9420013	12.4	0.1	3.7	0.5
Si III	1206.50	3550.041	0.005	1.9424293	13.20	0.04	10.3	0.4
Si III	1206.50	3550.269	0.004	1.9426184	13.46	0.05	9.1	0.3
H I	1215.67	3552.62	0.05	1.9223593	12.64	0.09	22	6
H I*	1215.67	3556.48	0.02	1.925527	17.1	0.2	25	1
H I*	1215.67	3557.4	0.1	1.92631	15.71	0.06	71	5
H I*	1215.67	3558.34	0.04	1.927060	15.4	0.1	18	4
H I*	1215.67	3559.38	0.02	1.927914	16.7	0.3	32	5
H I*	1215.67	3560.36	0.04	1.92872	15.53	0.07	30	1
H I	1215.67	3564.355	0.008	1.9320086	13.15	0.02	16	1
H I	1215.67	3565.43	0.02	1.9328904	15.0	0.2	20	1
H I	1215.67	3566.10	0.02	1.9334451	14.20	0.09	17	1
H I	1215.67	3570.22	0.01	1.9368323	13.08	0.03	22	2
H I*	1215.67	3574.445	(f)	1.9403086	13.38	0.02	24	1
H I*	1215.67	3574.958	(f)	1.9407306	13.39	0.03	16	1
H I*	1215.67	3575.292	(f)	1.9410052	13.2	0.1	18	3
H I*	1215.67	3576.293	(f)	1.9418286	13.76	0.05	67	19
H I*	1215.67	3576.499	(f)	1.9419981	15.51	0.07	23.2	0.7
H I*	1215.67	3577.029	(f)	1.9424342	16.0	0.1	35	1
H I*	1215.67	3577.258	(f)	1.9426225	15.9	0.1	14	2
H I	1215.67	3577.9	0.3	1.9431505	13.8	0.2	73	13
H I	1215.67	3584.87	0.04	1.9488864	12.84	0.05	35	4
H I	1215.67	3593.09	0.01	1.9556448	12.21	0.09	5	2

Table 2—Continued

ID	λ_{rest}	λ_{obs}	σ_λ	redshift	$\log N$	$\sigma_{\log N}$	b	σ_b
	Å	Å	Å				km s ⁻¹	km s ⁻¹
C IV	1548.19	3593.563	0.004	1.3211310	13.73	0.02	9.4	0.5
C IV	1548.19	3594.05	0.02	1.3214438	14.01	0.04	39	2
C IV	1548.19	3594.190	0.006	1.3215356	14.6	0.2	13	1
H I	1215.67	3597.64	0.02	1.9593898	13.53	0.03	29	2
H I	1215.67	3598.11	0.02	1.9597769	13.3	0.1	15	2
H I	1215.67	3598.46	0.06	1.9600643	13.1	0.1	22	5
C IV	1550.77	3599.540	0.004	1.3211310	13.73	0.02	9.4	0.5
C IV	1550.77	3600.03	0.02	1.3214439	14.01	0.04	39	2
C IV	1550.77	3600.168	0.006	1.3215357	14.6	0.2	13	1
H I	1215.67	3600.36	0.02	1.9616275	13.84	0.05	23	1
H I	1215.67	3601.09	0.02	1.9622270	12.45	0.09	12	3
H I	1215.67	3603.45	0.02	1.9641644	14.6	0.1	16	1
H I	1215.67	3604.04	0.02	1.9646504	14.13	0.05	21	1
H I	1215.67	3606.98	0.01	1.9670742	14.63	0.04	37	1
H I	1215.67	3607.84	0.08	1.9677832	12.6	0.2	19	9
H I	1215.67	3609.78	0.04	1.9693768	12.63	0.07	26	4
C IV	1548.19	3616.922	0.006	1.3362188	13.01	0.04	7.9	0.9
Si II	1260.42	3617.118	(f)	1.8697671	12.00	0.06	8	(f)
C IV	1548.19	3617.474	0.007	1.3365754	12.99	0.05	8	1
Si II	1260.42	3617.506	(f)	1.8700751	11.7	0.3	5.3	(f)
H I	1215.67	3617.72	0.03	1.9759055	12.6	0.1	14	4
C IV	1548.19	3618.07	0.01	1.3369629	12.96	0.05	10	1
Si II	1260.42	3618.145	(f)	1.8705820	11.4	0.3	4	(f)
C IV	1548.19	3618.743	0.004	1.3373952	13.00	0.03	5.4	0.5
H I	1215.67	3622.87	0.02	1.9801394	12.87	0.04	26	4
C IV	1550.77	3622.938	0.006	1.3362190	13.01	0.04	7.9	0.9
C IV	1550.77	3623.491	0.007	1.3365753	12.99	0.05	8	1
C IV	1550.77	3624.09	0.01	1.3369629	12.96	0.05	10	1
N V	1238.82	3624.44	(f)	1.925719	12.77	0.08	14	(f)
C IV	1550.77	3624.762	0.004	1.3373952	13.00	0.03	5.4	0.5
N V	1238.82	3624.78	(f)	1.925989	< 12.4	0.1	6.7	(f)
H I	1215.67	3627.85	0.01	1.9842420	13.37	0.02	35	1
H I	1215.67	3633.394	0.004	1.9887993	14.25	0.02	27.1	0.5
H I	1215.67	3634.985	0.005	1.9901085	13.70	0.01	22.2	0.6
H I	1215.67	3635.92	0.03	1.9908817	12.66	0.07	20	5
N V	1242.80	3636.10	(f)	1.925719	12.77	0.08	14	(f)

Table 2—Continued

ID	λ_{rest} Å	λ_{obs} Å	σ_λ Å	redshift	$\log N$	$\sigma_{\log N}$	b km s $^{-1}$	σ_b km s $^{-1}$
N V	1242.80	3636.43	(f)	1.925989	< 12.4	0.1	6.7	(f)
H I	1215.67	3637.14	0.01	1.9918828	13.47	0.01	30	1
H I	1215.67	3638.86	0.01	1.9932953	12.88	0.03	16	1
H I	1215.67	3641.804	0.008	1.9957179	13.38	0.01	24.6	0.8
H I	1215.67	3645.47	0.03	1.9987342	12.41	0.07	16	3
H I	1215.67	3654.895	0.008	2.0064862	13.34	0.02	21.3	0.9
H I	1215.67	3659.86	0.08	2.0105748	12.5	0.1	27	9
H I	1215.67	3660.789	0.005	2.0113347	13.85	0.01	26.7	0.7
H I	1215.67	3662.54	0.03	2.0127778	12.85	0.04	30	3
H I	1215.67	3668.80	0.03	2.0179224	12.59	0.06	20	3
H I	1215.67	3669.76	0.03	2.0187140	12.39	0.08	15	4
H I	1215.67	3670.89	0.02	2.0196431	12.44	0.07	14	3
H I	1215.67	3676.796	0.009	2.0245020	14.08	0.04	22.2	0.9
H I	1215.67	3677.36	0.02	2.0249646	13.4	0.5	16	7
H I	1215.67	3677.6	0.5	2.0251639	13.3	0.7	33	20
H I	1215.67	3679.231	0.009	2.0265050	13.26	0.02	25	1
H I	1215.67	3680.29	0.02	2.0273750	13.04	0.03	28	2
H I	1215.67	3686.3	0.1	2.0323551	13.1	0.7	25	7
H I	1215.67	3686.7	0.2	2.0326133	13.5	0.3	32	5
H I	1215.67	3687.51	0.03	2.0333130	13.07	0.08	27	5
Si II	1260.42	3687.933	0.005	1.9259506	12.26	0.03	7.6	0.6
H I	1215.67	3694.526	0.006	2.0390859	13.77	0.02	21.0	0.8
H I	1215.67	3694.8	0.1	2.0393157	13.1	0.1	55	8
H I	1215.67	3702.78	0.04	2.0458727	12.96	0.04	46	5
Si II	1260.42	3708.16	0.02	1.941996	11.75	0.09	10	3
Si II	1260.42	3708.72	0.02	1.942445	12.57	0.05	19	2
Si II	1260.42	3708.929	0.003	1.9426084	12.59	0.04	5.5	0.6
Si III	1206.50	3712.985	0.008	2.0774848	11.55	0.09	7.8	0.9
H I	1215.67	3719.298	0.006	2.0594633	13.67	0.01	31.7	0.7
H I	1215.67	3722.94	0.01	2.0624611	13.14	0.02	25	2
H I	1215.67	3723.79	0.02	2.0631599	12.91	0.04	25	2
H I	1215.67	3731.319	0.008	2.0693517	14.19	0.04	30	1
H I	1215.67	3731.46	0.05	2.0694718	13.6	0.1	53	4
H I	1215.67	3736.513	0.004	2.0736241	14.33	0.01	31.1	0.4
H I	1215.67	3737.505	0.009	2.0744402	13.52	0.07	18	1
H I	1215.67	3737.87	0.04	2.0747430	13.70	0.05	36	2

Table 2—Continued

ID	λ_{rest}	λ_{obs}	σ_λ	redshift	$\log N$	$\sigma_{\log N}$	b	σ_b
	Å	Å	Å				km s ⁻¹	km s ⁻¹
H I*	1215.67	3740.1	0.2	2.0765765	13.2	0.3	29	9
H I*	1215.67	3740.56	0.09	2.0769508	15.2	0.2	21	3
H I*	1215.67	3741.08	0.03	2.0773847	15.45	0.09	24.7	0.9
H I	1215.67	3743.716	0.005	2.0795491	14.62	0.06	16.2	0.6
H I	1215.67	3743.88	0.02	2.0796833	13.64	0.04	38	2
H I	1215.67	3752.808	0.004	2.0870287	13.92	0.01	28.3	0.4
H I	1215.67	3758.32	0.08	2.0915654	12.4	0.1	25	7
H I	1215.67	3759.05	0.04	2.0921648	12.79	0.06	28	5
H I	1215.67	3762.9	0.1	2.0952954	12.8	0.2	26	8
H I	1215.67	3763.37	0.02	2.0957181	13.55	0.04	24	1
H I	1215.67	3765.45	0.02	2.0974305	13.10	0.03	29	2
H I	1215.67	3769.98	0.01	2.1011577	13.15	0.02	20	1
H I	1215.67	3770.67	0.02	2.1017218	13.10	0.05	16	2
H I	1215.67	3771.12	0.02	2.1020923	13.15	0.04	17	2
H I	1215.67	3773.13	0.02	2.1037464	13.02	0.03	25	2
H I	1215.67	3776.079	0.008	2.1061709	13.61	0.01	23.7	0.9
H I	1215.67	3776.68	0.05	2.1066661	12.4	0.1	14	5
H I*	1215.67	3784.23	0.02	2.1128750	14.85	0.04	33.3	0.9
H I*	1215.67	3784.50	0.03	2.1130946	14.0	0.1	42	4
H I	1215.67	3788.61	0.01	2.1164834	13.08	0.02	19	1
H I	1215.67	3791.649	0.006	2.1189787	13.40	0.01	21.8	0.7
H I	1215.67	3792.96	0.04	2.1200564	12.69	0.09	22	5
H I	1215.67	3793.54	0.03	2.1205316	12.87	0.06	21	3
H I	1215.67	3811.377	0.008	2.1352067	13.47	0.01	28.3	0.8
H I	1215.67	3824.100	0.008	2.1456723	13.08	0.02	18.7	0.8
H I	1215.67	3825.370	0.007	2.1467175	13.42	0.01	26.3	0.8
H I	1215.67	3826.08	0.01	2.1473045	12.84	0.03	15	1
H I	1215.67	3828.28	0.02	2.1491120	13.4	0.1	22	1
H I	1215.67	3828.77	0.04	2.1495109	13.72	0.06	34	4
H I	1215.67	3829.560	0.007	2.1501641	13.70	0.02	20.1	0.8
C II	1334.53	3830.208	(f)	1.8700749	13.04	0.06	5.3	0.6
H I	1215.67	3830.30	0.03	2.1507692	13.30	0.04	37	3
C II	1334.53	3830.885	(f)	1.8705820	12.4	0.1	3	1
H I	1215.67	3835.17	0.03	2.1547759	12.55	0.06	19	3
H I	1215.67	3838.25	0.04	2.1573117	12.73	0.05	39	4
Si II	1304.37	3837.45	0.02	1.941996	11.75	0.09	10	3

Table 2—Continued

ID	λ_{rest}	λ_{obs}	σ_λ	redshift	$\log N$	$\sigma_{\log N}$	b	σ_b
	Å	Å	Å				km s ⁻¹	km s ⁻¹
Si II	1304.37	3838.04	0.02	1.942445	12.57	0.05	19	2
Si II	1304.37	3838.251	0.003	1.9426085	12.59	0.04	5.5	0.6
H I	1215.67	3843.02	0.01	2.1612370	12.94	0.02	23	1
C IV	1548.19	3843.830	0.006	1.4827815	13.16	0.03	7.0	0.6
C IV	1548.19	3844.10	0.01	1.4829553	12.96	0.05	11	2
C IV	1548.19	3844.437	0.006	1.4831734	12.80	0.06	4.3	0.9
C IV	1548.19	3844.751	0.007	1.4833764	12.99	0.08	5	1
C IV	1548.19	3844.80	0.01	1.4834117	13.58	0.03	21	1
H I	1215.67	3849.92	0.08	2.1669092	12.50	0.09	34	7
C IV	1550.77	3850.223	0.006	1.4827816	13.16	0.03	7.0	0.6
C IV	1550.77	3850.49	0.01	1.4829555	12.96	0.05	11	2
C IV	1550.77	3850.831	0.006	1.4831735	12.80	0.06	4.3	0.9
C IV	1550.77	3851.146	0.007	1.4833765	12.99	0.08	5	1
C IV	1550.77	3851.20	0.01	1.4834117	13.58	0.03	21	1
H I	1215.67	3851.23	0.02	2.1679876	13.04	0.03	32	2
H I	1215.67	3854.630	0.003	2.1707864	13.81	0.01	22.9	0.3
H I	1215.67	3862.60	0.03	2.1773462	12.79	0.04	35	3
H I	1215.67	3868.72	0.06	2.1823750	12.2	0.1	22	6
H I	1215.67	3869.86	0.01	2.1833181	12.98	0.02	24	1
H I	1215.67	3871.33	0.03	2.1845241	12.55	0.05	25	3
H I	1215.67	3873.52	0.02	2.1863263	13.02	0.02	33	2
H I	1215.67	3874.91	0.02	2.1874690	12.75	0.03	24	2
Si II	1260.42	3878.930	0.008	2.0774848	12.59	0.02	27	2
H I	1215.67	3881.208	0.005	2.1926489	13.43	0.01	24.7	0.5
H I	1215.67	3883.208	0.005	2.1942947	13.27	0.01	21.2	0.5
Si IV	1393.76	3884.700	0.005	1.7872190	12.01	0.06	6	1
H I*	1215.67	3887.513	(f)	2.1978357	12.64	0.06	26	3
H I*	1215.67	3887.953	(f)	2.1981976	13.59	0.01	36.4	0.7
H I	1215.67	3893.27	0.09	2.2025692	13.5	0.2	38	3
H I	1215.67	3893.59	0.02	2.2028329	13.87	0.08	32	1
H I	1215.67	3894.752	0.006	2.2037904	13.13	0.01	19.2	0.6
H I*	1215.67	3896.51	0.01	2.2052388	13.22	0.02	47	2
H I*	1215.67	3897.474	0.008	2.2060297	12.75	0.05	31	4
H I*	1215.67	3898.47	0.02	2.2068520	12.59	0.07	27	4
H I*	1215.67	3899.36	0.02	2.2075779	12.98	0.03	41	4
C II	1334.53	3904.46	0.01	1.925718	12.4	0.2	18	11

Table 2—Continued

ID	λ_{rest} Å	λ_{obs} Å	σ_λ Å	redshift	$\log N$	$\sigma_{\log N}$	b km s $^{-1}$	σ_b km s $^{-1}$
C II	1334.53	3904.776	0.005	1.9259505	12.91	0.05	7.6	0.6
Si IV	1402.77	3908.364	0.003	1.7861758	12.83	0.04	25	3
H I	1215.67	3909.875	0.003	2.2162304	13.86	0.01	25.2	0.3
H I	1215.67	3915.67	0.02	2.2210007	13.57	0.04	24	1
H I	1215.67	3916.41	0.02	2.2216103	13.80	0.06	36	5
H I	1215.67	3917.08	0.05	2.2221594	13.3	0.1	27	2
H I	1215.67	3918.80	0.01	2.2235696	12.80	0.03	19	1
H I	1215.67	3919.43	0.02	2.2240887	12.60	0.04	20	2
C II	1334.53	3925.97	0.06	1.941831	13.0	0.1	20	4
C II	1334.53	3926.21	0.01	1.942013	12.8	0.2	9	2
C II	1334.53	3926.85	0.01	1.942489	13.63	0.02	16.6	0.6
C II	1334.53	3927.017	0.002	1.9426165	13.50	0.03	5.2	0.4
Ca II	3934.78	3934.782	0.002	0.0000012	12.17	0.01	7.1	0.3
Ca II	3934.78	3935.66	0.05	0.0002236	12.00	0.07	31	6
Ca II	3934.78	3936.000	0.003	0.0003108	11.92	0.04	4.5	0.6
Ca II	3934.78	3936.28	0.01	0.0003828	11.54	0.08	8	1
H I	1215.67	3947.43	0.05	2.2471263	12.7	0.1	22	4
H I	1215.67	3948.0	0.2	2.2475970	12.2	0.3	26	14
Mg II	2796.35	3954.767	0.001	0.4142593	12.79	0.01	7.2	0.1
C IV	1548.19	3957.73	0.01	1.5563538	12.19	0.06	6	1
N V	1238.82	3960.86	0.01	2.1972857	12.87	0.04	19	2
N V	1238.82	3961.542	0.006	2.1978328	13.03	0.05	12	1
N V	1238.82	3961.992	0.002	2.1981955	14.25	0.00	34.0	0.4
C IV	1550.77	3964.32	0.01	1.5563540	12.19	0.06	6	1
Mg II	2803.53	3964.920	0.001	0.4142593	12.79	0.01	7.2	0.1
N V	1238.82	3965.54	0.03	2.2010598	13.25	0.04	43	3
N V	1238.82	3966.10	0.01	2.2015083	12.65	0.09	11	2
Ca II	3969.59	3969.596	0.002	0.0000012	12.17	0.01	7.1	0.3
Ca II	3969.59	3970.48	0.05	0.0002236	12.00	0.07	31	6
N V	1238.82	3970.72	0.01	2.2052388	14.24	0.01	92	1
Ca II	3969.59	3970.825	0.003	0.0003108	11.92	0.04	4.5	0.6
Ca II	3969.59	3971.11	0.01	0.0003829	11.54	0.08	8	1
N V	1238.82	3971.697	0.008	2.2060297	12.86	0.06	16	2
N V	1238.82	3972.72	0.02	2.2068520	13.30	0.06	34	3
N V	1242.80	3973.60	0.01	2.1972857	12.87	0.04	19	2
N V	1238.82	3973.61	0.02	2.2075779	13.75	0.02	54	3

Table 2—Continued

ID	λ_{rest}	λ_{obs}	σ_λ	redshift	$\log N$	$\sigma_{\log N}$	b	σ_b
	Å	Å	Å				km s ⁻¹	km s ⁻¹
N V	1242.80	3974.279	0.006	2.1978328	13.03	0.05	12	1
N V	1242.80	3974.730	0.002	2.1981955	14.25	0.00	34.0	0.4
N V	1242.80	3978.29	0.03	2.2010601	13.25	0.04	43	3
N V	1242.80	3978.85	0.01	2.2015085	12.65	0.09	11	2
N V	1242.80	3983.48	0.01	2.2052388	14.24	0.01	92	1
N V	1242.80	3984.466	0.008	2.2060297	12.86	0.06	16	2
N V	1242.80	3985.49	0.02	2.2068520	13.30	0.06	34	3
N V	1242.80	3986.39	0.03	2.2075777	13.75	0.02	54	3
Si IV	1393.76	3996.584	0.001	1.8674941	12.97	0.01	5.3	0.1
Si IV	1393.76	3996.938	0.003	1.8677480	12.49	0.02	4.6	0.4
Si IV	1393.76	3997.93	0.01	1.8684596	11.6	0.1	3	3
Si IV	1393.76	3999.58	0.07	1.8696406	12.3	0.1	23	4
Si IV	1393.76	3999.753	0.002	1.8697674	13.12	0.02	6.6	0.2
Si IV	1393.76	4000.182	0.004	1.8700752	12.72	0.02	8.3	0.6
Si IV	1393.76	4000.40	0.01	1.8702323	12.01	0.08	4	1
Si IV	1393.76	4000.65	0.01	1.8704109	11.6	0.1	3	2
Si IV	1393.76	4000.888	0.004	1.8705820	12.24	0.03	4.2	0.5
Si IV	1393.76	4001.581	0.002	1.8710794	12.86	0.01	8.6	0.2
Si IV	1393.76	4002.581	0.008	1.8717965	12.03	0.05	6	1
C IV	1548.19	4010.680	0.005	1.5905522	13.39	0.03	8.4	0.4
C IV	1548.19	4010.92	0.02	1.5907099	13.07	0.05	11	1
C IV	1550.77	4017.351	0.005	1.5905523	13.39	0.03	8.4	0.4
C IV	1550.77	4017.59	0.02	1.5907100	13.07	0.05	11	1
Si IV	1402.77	4022.434	0.001	1.8674937	12.97	0.01	5.3	0.1
Si IV	1402.77	4022.791	0.003	1.8677479	12.49	0.02	4.6	0.4
Si IV	1402.77	4023.79	0.01	1.8684596	11.6	0.1	3	3
Si IV	1402.77	4025.45	0.07	1.8696405	12.3	0.1	23	4
Si IV	1402.77	4025.624	0.002	1.8697673	13.12	0.02	6.6	0.2
Si IV	1402.77	4026.055	0.004	1.8700750	12.72	0.02	8.3	0.6
Si IV	1402.77	4026.28	0.01	1.8702322	12.01	0.08	4	1
Si IV	1402.77	4026.53	0.01	1.8704109	11.6	0.1	3	2
Si IV	1402.77	4026.766	0.004	1.8705819	12.24	0.03	4.2	0.5
Si IV	1402.77	4027.464	0.002	1.8710794	12.86	0.01	8.6	0.2
Si IV	1402.77	4028.470	0.008	1.8717965	12.03	0.05	6	1
Si IV	1393.76	4077.33	0.04	1.925429	11.7	0.2	11	5
Si IV	1393.76	4077.74	0.01	1.925719	12.24	0.05	14	1

Table 2—Continued

ID	λ_{rest} Å	λ_{obs} Å	σ_λ Å	redshift	$\log N$	$\sigma_{\log N}$	b km s $^{-1}$	σ_b km s $^{-1}$
Si IV	1393.76	4078.112	0.002	1.925989	12.72	0.01	6.7	0.2
Si IV	1393.76	4100.393	0.006	1.9419751	12.78	0.03	14.3	0.7
Si IV	1393.76	4100.429	0.003	1.9420015	12.66	0.04	3.7	0.5
Si IV	1393.76	4101.025	0.006	1.9424292	13.34	0.02	10.3	0.4
Si IV	1393.76	4101.289	0.004	1.9426184	13.39	0.02	9.1	0.3
Si IV	1402.77	4103.70	0.03	1.925429	11.7	0.2	11	5
Si IV	1402.77	4104.11	0.01	1.925719	12.24	0.05	14	1
Si IV	1402.77	4104.490	0.002	1.925989	12.72	0.01	6.7	0.2
Si IV	1402.77	4126.914	0.006	1.9419751	12.78	0.03	14.3	0.7
Si IV	1402.77	4126.951	0.003	1.9420015	12.66	0.04	3.7	0.5
Si IV	1402.77	4127.551	0.006	1.9424292	13.34	0.02	10.3	0.4
Si IV	1402.77	4127.816	0.004	1.9426184	13.39	0.02	9.1	0.3
C IV	1548.19	4229.12	0.01	1.7316473	12.53	0.05	8	1
C IV	1550.77	4236.16	0.01	1.7316473	12.53	0.05	8	1
C IV	1548.19	4313.543	0.003	1.7861758	13.92	0.01	24.8	0.3
C IV	1548.19	4314.60	0.02	1.7868581	12.71	0.06	16	3
C IV	1548.19	4315.159	0.005	1.7872192	13.26	0.02	12.2	0.6
C IV	1550.77	4320.718	0.003	1.7861761	13.92	0.01	24.8	0.3
C IV	1550.77	4321.78	0.02	1.7868583	12.71	0.06	16	3
C IV	1550.77	4322.336	0.005	1.7872192	13.26	0.02	12.2	0.6
C IV	1548.19	4358.65	0.02	1.8153124	12.38	0.09	10	3
C IV	1548.19	4359.18	0.02	1.8156517	12.76	0.04	16	2
C IV	1550.77	4365.90	0.02	1.8153123	12.38	0.09	10	3
C IV	1550.77	4366.43	0.02	1.8156517	12.76	0.04	16	2
Si II	1526.71	4381.76	(f)	1.8700752	12.09	0.09	5.3	(f)
Mg II	2796.35	4390.42	0.04	0.5700546	12.12	0.08	16	3
Mg II	2796.35	4390.754	0.008	0.5701721	12.28	0.05	7.7	0.8
Mg II	2796.35	4391.57	0.01	0.5704634	11.49	0.07	2	1
Mg II	2803.53	4401.70	0.04	0.5700546	12.12	0.08	16	3
Mg II	2803.53	4402.026	0.008	0.5701722	12.28	0.05	7.7	0.8
Mg II	2803.53	4402.84	0.01	0.5704634	11.49	0.07	2	1
Mg II	2796.35	4418.458	0.008	0.5800791	12.49	0.02	14	1
Mg II	2796.35	4418.87	0.01	0.5802267	11.96	0.05	7	1
Mg II	2803.53	4429.801	0.008	0.5800791	12.49	0.02	14	1
Mg II	2803.53	4430.21	0.01	0.5802268	11.96	0.05	7	1
C IV	1548.19	4439.26	0.08	1.8673762	13.37	0.08	52	5

Table 2—Continued

ID	λ_{rest}	λ_{obs}	σ_λ	redshift	$\log N$	$\sigma_{\log N}$	b	σ_b
	Å	Å	Å				km s ⁻¹	km s ⁻¹
C IV	1548.19	4439.438	0.004	1.8674929	13.7	0.1	5	1
C IV	1548.19	4439.48	0.07	1.8675234	13.53	0.06	17	8
C IV	1548.19	4439.849	0.005	1.8677584	13.84	0.04	6.4	0.4
C IV	1548.19	4440.16	0.01	1.8679577	12.2	0.1	4	2
C IV	1548.19	4440.93	0.01	1.8684571	12.57	0.05	9	2
C IV	1548.19	4441.382	0.009	1.8687488	12.77	0.04	7.8	0.9
C IV	1548.19	4441.718	0.004	1.8689657	13.12	0.02	8.4	0.5
C IV	1548.19	4442.412	0.007	1.8694136	12.5	0.2	1.6	0.8
C IV	1548.19	4442.72	0.02	1.8696114	13.62	0.04	18	1
C IV	1548.19	4442.978	0.004	1.8697791	13.55	0.05	7.7	0.5
C IV	1548.19	4443.414	0.006	1.8700610	13.33	0.07	12	1
C IV	1548.19	4443.7	0.1	1.8702604	13.1	0.1	33	7
C IV	1548.19	4444.217	0.004	1.8705796	12.94	0.06	6.2	0.9
C IV	1548.19	4445.023	0.002	1.8711005	13.68	0.01	9.9	0.2
C IV	1548.19	4446.118	0.003	1.8718073	13.20	0.02	7.0	0.3
C IV	1548.19	4446.35	0.09	1.8719591	13.14	0.05	69	10
C IV	1550.77	4446.64	0.08	1.8673762	13.37	0.08	52	5
C IV	1550.77	4446.822	0.004	1.8674928	13.7	0.1	5	1
C IV	1550.77	4446.87	0.07	1.8675236	13.53	0.06	17	8
C IV	1550.77	4447.234	0.005	1.8677585	13.84	0.04	6.4	0.4
C IV	1550.77	4447.54	0.01	1.8679578	12.2	0.1	4	2
C IV	1550.77	4448.32	0.01	1.8684572	12.57	0.05	9	2
C IV	1550.77	4448.770	0.009	1.8687488	12.77	0.04	7.8	0.9
C IV	1550.77	4449.106	0.004	1.8689656	13.12	0.02	8.4	0.5
C IV	1550.77	4449.801	0.007	1.8694137	12.5	0.2	2	0.8
C IV	1550.77	4450.11	0.02	1.8696115	13.62	0.04	18	1
C IV	1550.77	4450.368	0.004	1.8697792	13.55	0.05	7.7	0.5
C IV	1550.77	4450.805	0.006	1.8700614	13.33	0.07	12	1
C IV	1550.77	4451.1	0.1	1.8702604	13.1	0.1	33	7
C IV	1550.77	4451.609	0.004	1.8705797	12.94	0.06	6.2	0.9
C IV	1550.77	4452.417	0.002	1.8711004	13.68	0.01	9.9	0.2
C IV	1550.77	4453.513	0.003	1.8718077	13.20	0.02	7.0	0.3
C IV	1550.77	4453.75	0.09	1.8719591	13.14	0.05	69	10
Si II	1526.71	4491.56	0.03	1.941996	11.75	0.09	10	3
Si II	1526.71	4492.25	0.03	1.942446	12.57	0.05	19	2
Si II	1526.71	4492.500	0.004	1.9426084	12.59	0.04	5.5	0.6

Table 2—Continued

ID	λ_{rest}	λ_{obs}	σ_λ	redshift	$\log N$	$\sigma_{\log N}$	b	σ_b
	Å	Å	Å				km s ⁻¹	km s ⁻¹
C IV	1548.19	4529.13	0.05	1.925429	12.2	0.1	11	5
C IV	1548.19	4529.58	0.01	1.925718	13.07	0.03	14	1
C IV	1548.19	4530.001	0.002	1.925989	13.41	0.01	7.0	0.2
C IV	1550.77	4536.67	0.05	1.925429	12.2	0.1	11	5
C IV	1550.77	4537.12	0.01	1.925718	13.07	0.03	14	1
C IV	1550.77	4537.536	0.002	1.9259888	13.41	0.01	7.0	0.2
C IV	1548.19	4552.17	0.02	1.9403086	12.67	0.04	12	1
C IV	1548.19	4552.824	0.004	1.9407302	12.97	0.02	7.0	0.4
C IV	1548.19	4553.250	0.009	1.9410059	12.78	0.03	10	1
C IV	1548.19	4554.467	0.006	1.9417915	12.98	0.05	5.8	0.6
C IV	1548.19	4554.75	(f)	1.941974	13.89	0.01	16.4	0.6
C IV	1548.19	4555.15	(f)	1.942233	12.84	0.08	5	1
C IV	1548.19	4555.45	(f)	1.942427	14.01	0.03	10.1	0.4
C IV	1548.19	4555.75	(f)	1.942618	14.1	0.1	14	1
C IV	1548.19	4555.85	0.05	1.942686	13.8	0.2	18	1
C IV	1550.77	4559.74	0.02	1.9403088	12.67	0.04	12	1
C IV	1550.77	4560.396	0.004	1.9407303	12.97	0.02	7.0	0.4
C IV	1550.77	4560.824	0.009	1.9410062	12.78	0.03	10	1
C IV	1550.77	4562.042	0.006	1.9417915	12.98	0.05	5.8	0.6
C IV	1550.77	4562.33	(f)	1.941974	13.89	0.01	16.4	0.6
C IV	1550.77	4562.73	(f)	1.942233	12.84	0.08	5	1
C IV	1550.77	4563.03	(f)	1.942427	14.01	0.03	10.1	0.4
C IV	1550.77	4563.32	(f)	1.942618	14.1	0.1	14	1
C IV	1550.77	4563.43	0.05	1.942686	13.8	0.2	18	1
Mg II	2796.35	4599.938	0.003	0.6449782	12.34	0.02	3.2	0.4
Mg II	2803.53	4611.748	0.003	0.6449783	12.34	0.02	3.2	0.4
C IV	1548.19	4764.24	0.01	2.0772858	12.98	0.05	11	1
C IV	1548.19	4764.55	0.01	2.0774848	12.90	0.05	7.8	0.9
C IV	1550.77	4772.16	0.01	2.0772858	12.98	0.05	11	1
C IV	1550.77	4772.47	0.01	2.0774848	12.90	0.05	7.8	0.9
Al II	1670.79	4794.771	(f)	1.8697671	11.1	0.2	7	4
Al II	1670.79	4795.285	(f)	1.8700751	11.0	0.1	5.3	0.6
C IV	1548.19	4819.34	0.02	2.1128747	12.60	0.07	31	6
C IV	1548.19	4819.68	0.04	2.1130946	12.0	0.1	8	2
C IV	1550.77	4827.35	0.02	2.1128750	12.60	0.07	31	6
C IV	1550.77	4827.69	0.04	2.1130946	12.0	0.1	8	2

Table 2—Continued

ID	λ_{rest} Å	λ_{obs} Å	σ_λ Å	redshift	$\log N$	$\sigma_{\log N}$	b km s $^{-1}$	σ_b km s $^{-1}$
Mg II	2796.35	4902.38	0.02	0.7531351	11.27	0.08	6	2
Mg II	2803.53	4914.97	0.02	0.7531351	11.27	0.08	6	2
Al III	1670.79	4916.27	0.01	1.942489	11.39	0.05	16.6	0.6
Al III	1670.79	4916.486	0.003	1.9426165	11.21	0.06	5.2	0.4
C IV	1548.19	4950.02	0.01	2.1972857	12.63	0.05	30	5
C IV	1548.19	4950.869	0.008	2.1978328	12.49	0.06	7	1
C IV	1548.19	4951.430	0.003	2.1981955	13.91	0.00	25.0	0.3
C IV	1548.19	4955.86	0.04	2.2010598	12.91	0.03	43	3
C IV	1548.19	4956.56	0.02	2.2015083	12.27	0.09	11	2
C IV	1550.77	4958.25	0.01	2.1972857	12.63	0.05	30	5
C IV	1550.77	4959.104	0.008	2.1978331	12.49	0.06	7	1
C IV	1550.77	4959.666	0.003	2.1981957	13.91	0.00	25.0	0.3
C IV	1548.19	4962.33	0.01	2.2052388	13.99	0.01	83	1
C IV	1548.19	4963.56	0.01	2.2060297	13.25	0.02	27	1
C IV	1548.19	4964.83	0.02	2.2068520	13.45	0.03	36	2
C IV	1548.19	4965.96	0.03	2.2075779	13.57	0.02	51	2
C IV	1550.77	4970.59	0.01	2.2052386	13.99	0.01	83	1
C IV	1550.77	4971.81	0.01	2.2060294	13.25	0.02	27	1
C IV	1550.77	4973.09	0.02	2.2068520	13.45	0.03	36	2
C IV	1550.77	4974.22	0.03	2.2075779	13.57	0.02	51	2
Al III	1854.72	5457.48	0.01	1.942489	11.92	0.05	16.6	0.6
Al III	1854.72	5457.719	0.003	1.9426166	11.79	0.05	5.2	0.4
Al III	1862.79	5481.24	0.01	1.942489	11.92	0.05	16.6	0.6
Al III	1862.79	5481.475	0.003	1.9426166	11.79	0.05	5.2	0.4
Fe II	2382.77	5532.020	0.006	1.3216810	11.80	0.06	2.7	0.6
Fe II	2382.77	5532.22	0.01	1.3217632	11.5	0.1	5	1
Na I	5891.58	5891.572	0.005	-0.000002	11.72	0.02	6.5	0.4
Na I	5897.56	5897.546	0.005	-0.000002	11.72	0.02	6.5	0.4
Fe II	2600.17	6036.772	0.006	1.3216810	11.76	0.07	2.7	0.6
Fe II	2600.17	6036.98	0.01	1.3217630	11.5	0.1	5	1
Mg II	2796.35	6491.6	0.1	1.3214581	11.5	0.2	20	11
Mg II	2796.35	6492.237	0.007	1.3216809	11.92	0.04	2.7	0.6
Mg II	2796.35	6492.47	0.01	1.3217632	11.76	0.05	5	1
Mg II	2803.53	6508.905	0.007	1.3216810	11.92	0.04	2.7	0.6
Mg II	2803.53	6509.13	0.01	1.3217633	11.76	0.05	5	1
Mg II	2796.35	6532.890	(f)	1.3362187	11.67	0.06	16	3

Table 2—Continued

ID	λ_{rest} Å	λ_{obs} Å	σ_λ Å	redshift	$\log N$	$\sigma_{\log N}$	b km s $^{-1}$	σ_b km s $^{-1}$
Mg II	2796.35	6533.887	(f)	1.3365753	11.65	0.04	4.4	0.8
Mg II	2803.53	6549.662	(f)	1.3362190	11.67	0.06	16.5	3
Mg II	2803.53	6550.662	(f)	1.3365754	11.65	0.04	4.4	0.8
Fe II	2382.77	7332.45	0.02	2.0772858	11.7	0.2	11	1
Mg II	2796.35	8024.879	(f)	1.8697671	11.89	0.04	8	1
Mg II	2796.35	8025.740	(f)	1.8700750	11.97	0.03	5.3	0.6
Mg II	2796.35	8027.158	(f)	1.8705821	11.4	0.1	4	4
Mg II	2803.53	8045.481	(f)	1.8697672	11.89	0.04	8	1
Mg II	2803.53	8046.344	(f)	1.8700750	11.97	0.03	5.3	0.6
Mg II	2803.53	8047.766	(f)	1.8705822	11.4	0.1	4	4
Mg II	2796.35	8181.99	0.01	1.925950	11.72	0.08	7.6	0.6
Mg II	2803.53	8202.99	0.01	1.925950	11.72	0.08	7.6	0.6
Mg II	2796.35	8228.23	(f)	1.942489	12.54	(f)	16.6	(f)
Mg II	2796.35	8228.59	(f)	1.9426166	12.37	(f)	5.2	(f)
Mg II	2803.53	8249.36	0.02	1.942489	12.54	0.04	16.6	0.6
Mg II	2803.53	8249.717	0.004	1.9426166	12.37	0.05	5.2	0.4

Note. — An “*” marks the H I lines belonging to metal systems while the “(f)” stands for *fixed* and indicates that the line has been fitted imposing the redshift and/or the Doppler parameter value.

Table 3. List of metal absorption systems

redshift ^a	$\log N(\text{H I})^{\text{b}}$	$\log N(\text{Si IV})^{\text{b}}$	$\log N(\text{C IV})^{\text{b}}$	$\log N(\text{Mg II})^{\text{b}}$	# ^c
-0.000002 ^d	1
0.0002 ^e	4
0.41426	12.79	1
0.57017	12.55	3
0.58008	12.60	2
0.64498	12.34	1
0.75313	11.27	1
1.09169	13.53	< 11.3	1
1.32153	...	13.25	14.74	12.24	3
1.3368	...	blend	13.59	11.96	4
1.4831	...	blend	13.89	< 11.2	5
1.55635	14.11	< 11.7	12.19	< 11.2	1
1.59055	14.1	< 11.7	13.56	< 11.3	2
1.73165	14.10	< 11.6	12.53	< 11.6	1
1.78618	15.54	12.89	14.03	< 11.3	3
1.81565	15.15	< 11.4	12.91	< 11.4	2
1.8693	15.92	13.65	14.60	12.29	17
1.92599	17.3	12.87	13.59	11.72	3
1.9422	16.33	13.76	14.60	12.76	9
2.07729	15.64	< 11.5	13.24	...	2
2.11287	14.91	< 11.5	12.7	...	2
2.19819 ^f	13.64	< 12.1	13.95	< 11.2	3
2.20106 ^f	< 11.5	< 11.6	13.	< 11.2	2
2.2064 ^f	13.55	< 11.5	14.26	< 11.2	4

^aSee definition in §5^bLogarithmic total column density^cNumber of components fitted to the C IV absorption feature or to the Mg II absorption feature, if C IV is not observed^dGalactic Na I $\lambda\lambda$ 5891, 5897^eGalactic Ca II $\lambda\lambda$ 3934, 3969^fAssociated systems

REFERENCES

- Casertano, S., de Mello, D., Dickinson, M., Ferguson, H.C., Fruchter, A.S., et al. 2000, in preparation
- D'Odorico, V., Petitjean, P. 2000, in preparation
- Dekker, H., D'Odorico, S., Kaufer, A. 2000, SPIE, 4008, in press
- Fontana, A., Ballester, P. 1995, ESO The Messenger, 80, 37
- Fruchter, A.S. et al. 2000, in preparation
- Gardner, J.P., Baum, S.A., Brown, T.M., Carollo, C.M., Christensen, J., et al. 2000, AJ, 119, 486
- Giallongo, E., Cristiani, S., D'Odorico, S., Fontana, A., Savaglio, S. 1996, ApJ, 466, 64
- Hu, E.M., Kim., T., Cowie, L.L., Songaila, A., Rauch, M. 1995, AJ, 110, 1526
- Kirkman, D., Tytler, D., 1997, ApJ, 484, 672
- Lu, L., Sargent, W.L.W., Womble, D.S., Takada-Hidai, M. 1996, ApJ, 472, 509
- Lucas, R.A., et al. 2000, in preparation
- Morton, D.C. 1991, ApJS, 77, 119
- Outram, P.J., Boyle, B.J., Carswell, R.F., Hewett, P.C., Williams, R.E. 1999, MNRAS, 305, 685, OUT99
- Savaglio, S. 1998, AJ, 116, 1055, SAV98
- Savaglio, S., Ferguson, H.C., Brown, T.M., Espey, B.R., Sahu, K.C., Baum, S.A., Carollo, C.M., Kaiser, M.E., Stiavelli, M., Williams, R.E., Wilson, J. 1999, ApJ, 515, L5
- Sealey, K.M., Drinkwater, M.J., Webb, J.K. 1998, ApJ, 499, L135
- Tresse, L., Dennefeld, M., Petitjean, P., Cristiani, S., White, S. 1999, A&A, 346, 21L
- Verner, D. A., Barthel, P. D., Tytler, D. 1994, A&AS, 108, 287
- Weymann, R.J., Jannuzzi, B.T., Lu, L. et al. 1998, ApJ, 506, 1
- Williams, R.E., Baum, S., Bergeron, L.E., Bernstein, N., Blacker, B.S., et al. 2000, submitted to AJ

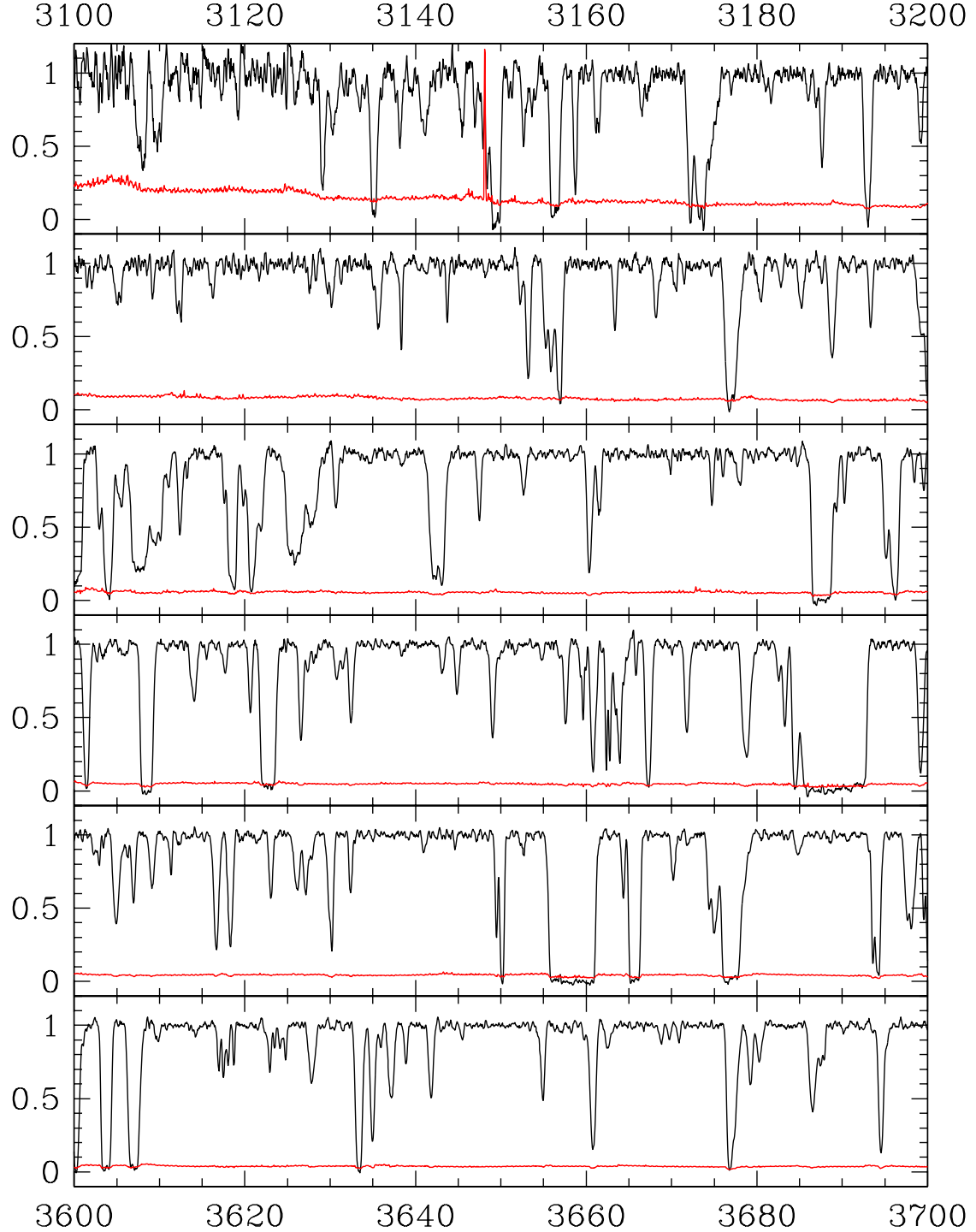


Fig. 1.— The normalized spectrum of J2233-606, plotted against vacuum heliocentric wavelength (\AA). Each panel contains a strip of 100 \AA with the wavelength increasing from the top to the bottom. The 1 σ error level is also shown.

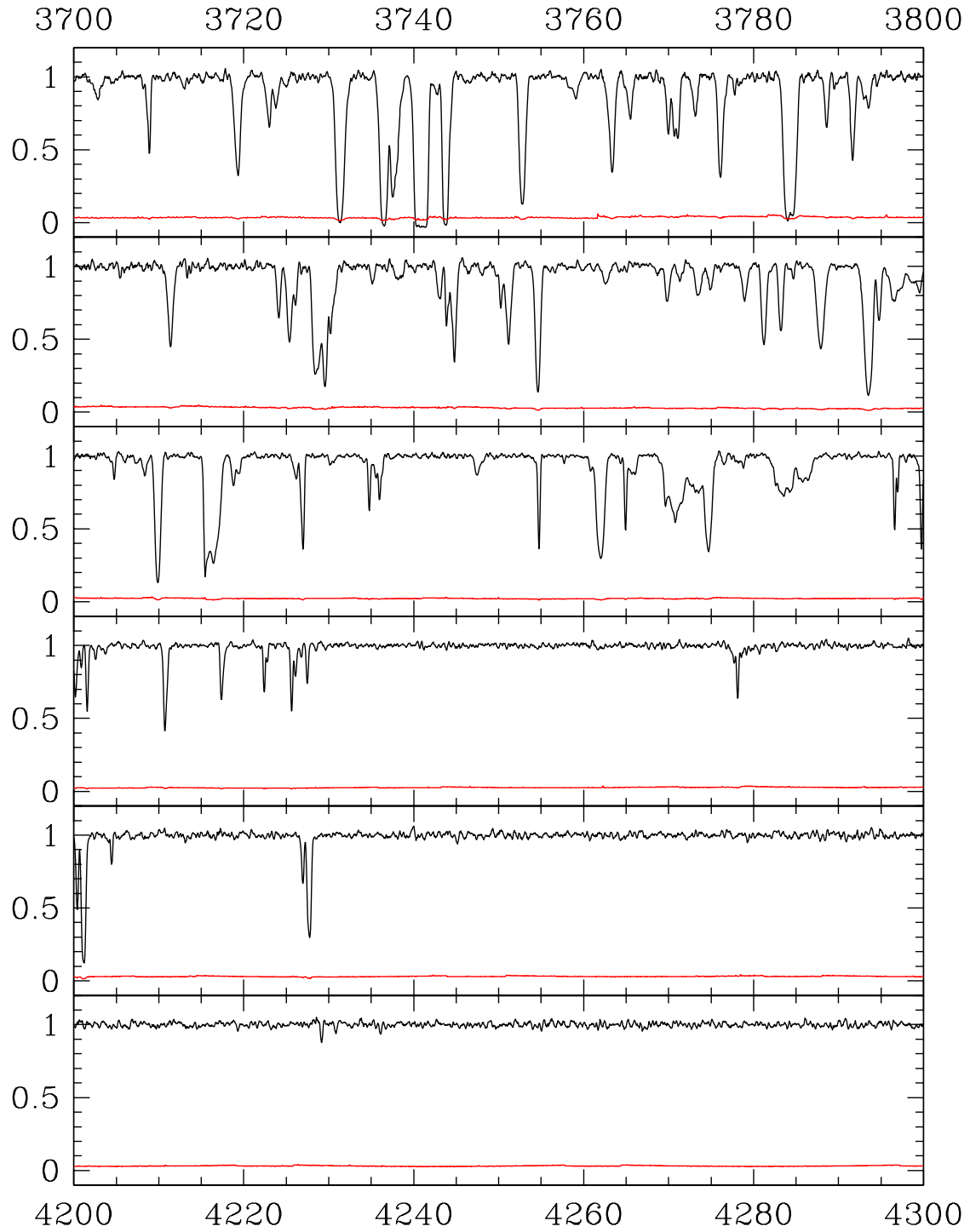


Fig. 2.— The normalized spectrum of J2233-606, plotted against vacuum heliocentric wavelength (\AA). Details as in Fig. 1.

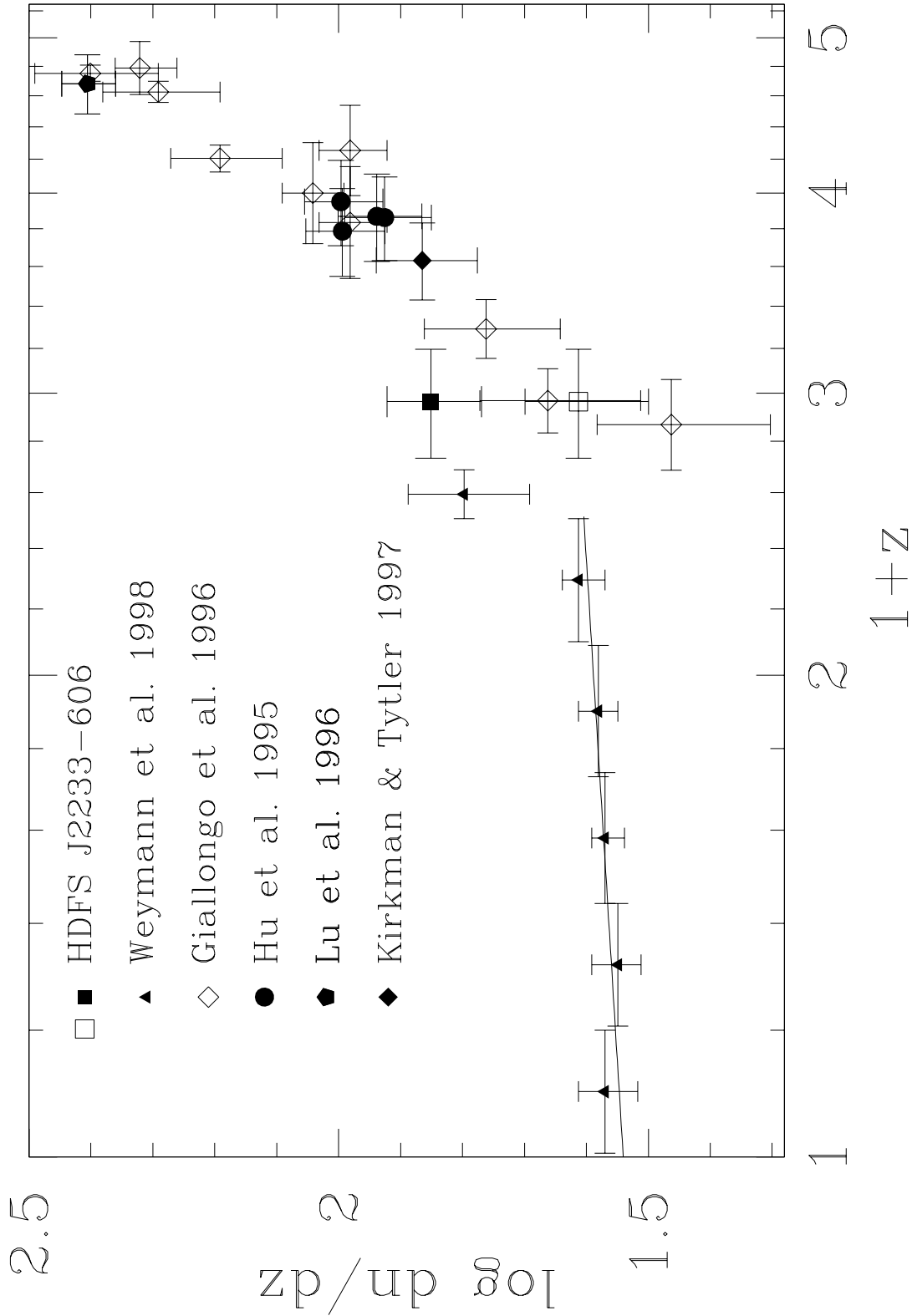


Fig. 3.— Number density evolution of the Ly α clouds with $\log N(\text{H I}) > 14$ from $z = 0$ to $z = 4$. Filled symbols are for samples that include metal systems, open symbols do not. The low-redshift line is the fit $dn/dz \propto (1+z)^{0.16}$ derived from a sample pf Ly α absorbers with equivalent width $EW \geq 0.24 \text{ \AA}$ (Weymann et al. 1998) which correspond to $\log N(\text{H I}) > 14$ for $b \sim 26 \text{ km s}^{-1}$.